

# Multistep Thermal Decomposition of Granular Sodium Perborate Tetrahydrate: A Kinetic Approach to Complex Reactions in Solid–Gas Systems

Nobuyoshi Koga,\* Nao Kameno, Yoji Tsuboi, Takayuki Fujiwara, Masayuki Nakano, Kazuyuki Nishikawa, and Akiko Iwasaki Murata

Department of Science Education, Graduate School of Education, Hiroshima University, 1-1-1 Kagamiyama, Higashi-Hiroshima, 739-8524 Japan

\* Corresponding Author. Tel/Fax: +81824247092; e-mail: [nkoga@hiroshima-u.ac.jp](mailto:nkoga@hiroshima-u.ac.jp)

## Contents

S1. Instrumental Calibration and Baseline Correction for Thermal Analyses .....	S1
S2. Characterization of Sample.....	S1
S3. Kinetics of the Thermal Dehydration Process .....	S2
S4. Kinetics of the thermal decomposition process .....	S4
References .....	S7

### S1. Instrumental Calibration and Baseline Correction for Thermal Analyses

The DSC instrument (DSC60) used in this study was calibrated in terms of temperature and enthalpy change by measuring the melting peaks of pure metals, including Ga, In, Sn, Pb, and Zn (>99.99% purity, Nilaco) at  $\beta = 5 \text{ K min}^{-1}$  under the same atmospheric conditions that applied to the sample measurements. Temperature calibration for TG–DTA instruments (DTG-50M and TG8120) was also carried out measuring melting points of the above pure metals and also of Al and Ag (>99.99% purity, Nilaco) at  $5 \text{ K min}^{-1}$ . For the suspension-type TG (TGA-50), temperature calibration was made with reference to the dropping temperatures of a platinum weight (10 mg) suspended from the sample holder by different pure metal wires, including In, Sn, Pb, Zn, Al, and Ag wires (>99.99% purity, Nilaco), during heating at  $\beta = 5 \text{ K min}^{-1}$  in flowing  $\text{N}_2$  ( $80 \text{ cm}^3 \text{ min}^{-1}$ ). In all the TG instruments, calibration of mass-change measurement was performed at room temperature by addition/removal of a 10 mg standard weight to the sample holder in the balance system. Subsequently, the correctness of the mass-change value at the higher temperatures were evaluated by the measurement of TG curve for the thermal dehydration and decomposition of calcium oxalate monohydrate (99.9985% purity, Alfa Aesar) at  $\beta = 5 \text{ K min}^{-1}$  under the same atmospheric conditions as those applied to sample measurement. For the TG–DTA measurements using the DTG-50M instrument, 5.00 mg of  $\text{Al}_2\text{O}_3$  weighed into a platinum pan paired with that for the sample was used as a reference for DTA and also as the counterbalance for TG. For the TG–DTA measurements using the TG/DTA–MS system, an empty platinum pan paired with that for the sample was used as the reference for DTA and the

counterbalance for TG. All the TG curves recorded were subjected to baseline correction using blank TG curves recorded using an empty platinum sample pan as the sample under the same measurement conditions as those applied to respective sample measurements, and subsequently smoothed via the moving average method of 5 points.

### S2. Characterization of Sample

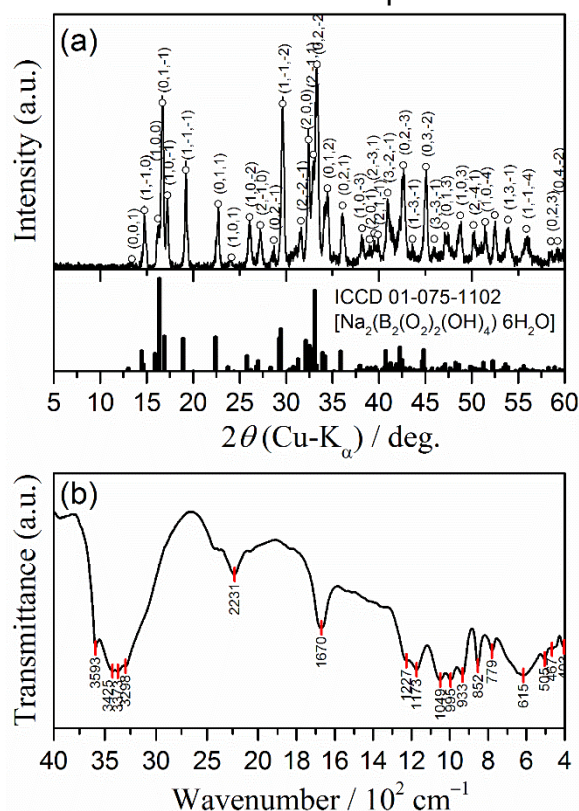
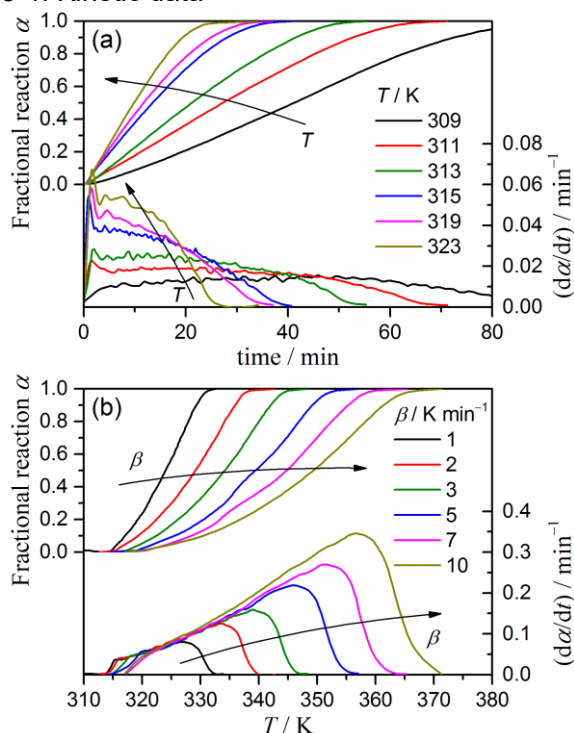


Figure S1. Structural characterization of the sample: (a) XRD pattern and (b) FTIR spectrum.

### S3. Kinetics of the Thermal Dehydration Process

#### S3-1. Kinetic data



**Figure S2.** Kinetic data for the thermal dehydration of SPB-4AQ recorded under (a) isothermal (selected) and (b) nonisothermal conditions in flowing  $N_2$  ( $80 \text{ cm}^3 \text{ min}^{-1}$ ).

#### S3-2. Mathematical deconvolution

Mathematical deconvolution of the DTG curves for the thermal dehydration process was performed using PeakFit 4.12. Assuming a three step reaction, the DTG curves were fitted by Weibull functions.<sup>S1</sup>

$$y = \left[ a_0 \left( \frac{a_3 - 1}{a_3} \right)^{\frac{1-a_3}{a_3}} \left\{ \frac{x - a_1}{a_2} + \left( \frac{a_3 - 1}{a_3} \right)^{\frac{1}{a_3}} \right\}^{a_3 - 1} \right] \exp \left[ - \left\{ \frac{x - a_1}{a_2} + \left( \frac{a_3 - 1}{a_3} \right)^{\frac{1}{a_3}} \right\}^{a_3} + \frac{a_3 - 1}{a_3} \right] \quad (\text{S1})$$

where  $a_0$ ,  $a_1$ ,  $a_2$ , and  $a_3$  index the amplitude, center, width, and shape.

Figure S3 shows typical results of a mathematical deconvolution of the DTG curves. From the ratio of the separated peak areas, the contributions  $c$  of each reaction step  $i$  to the overall thermal dehydration process were roughly estimated to be  $(c_1, c_2, c_3) = (0.10 \pm 0.01, 0.36 \pm 0.03, 0.54 \pm 0.03)$  as the average values for the kinetic data at different  $\beta$ . Furthermore, the separated kinetic data at different  $\beta$  can be used for calculating the apparent kinetic parameters of each reaction step. As shown in Figure S4, the kinetic data separated for each reaction step vary systematically with  $\beta$ .

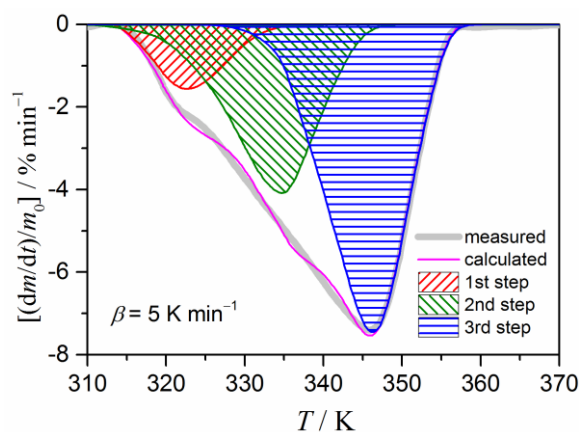


**Figure S3.** Typical results of a mathematical deconvolution of the DTG curves for the thermal dehydration process using the Weibull function.

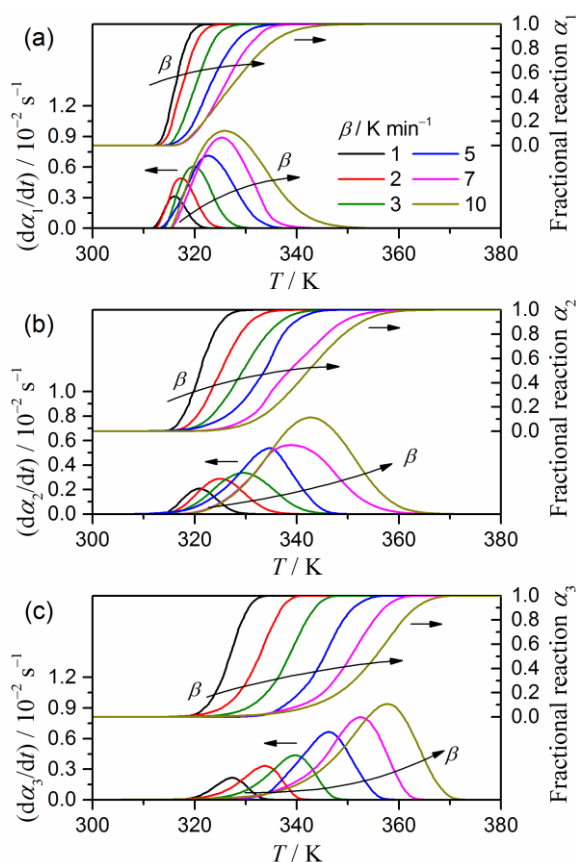


**Figure S4.** Kinetic data for each reaction step of the thermal dehydration process separated by mathematical deconvolution: (a) first step, (b) second step, and (c) third step.

#### S3-3. Formal kinetic analysis

Applying Friedman plots<sup>S2</sup> to the separated kinetic data, acceptable linearity for the  $\ln(d\alpha/dt)$  versus  $T^{-1}$  plots are evidenced irrespective of  $\alpha_i$  for each reaction step  $i$  (Figure S5). The slopes of the Friedman plots at different  $\alpha$  are practically identical in each reaction step for the second and third reaction steps, while a systematic change in the slope as the reaction advances is observed for the first reaction step. The  $E_a$  variations for each reaction step are shown in Figure S6. For the first reaction step, a systematic decrease in  $E_a$  from

approximately 250 to 50 kJ mol<sup>-1</sup> is observed as the reaction advances, which is indicative of a change in rate behavior during the course of the first reaction step. Conversely, the  $E_a$  values for the second and third reaction steps are practically constant during the course of the reaction, with the averaged values of  $54.8 \pm 4.5$  kJ mol<sup>-1</sup> and  $49.1 \pm 0.6$  kJ mol<sup>-1</sup> in the range  $0.1 \leq \alpha \leq 0.9$ , respectively.

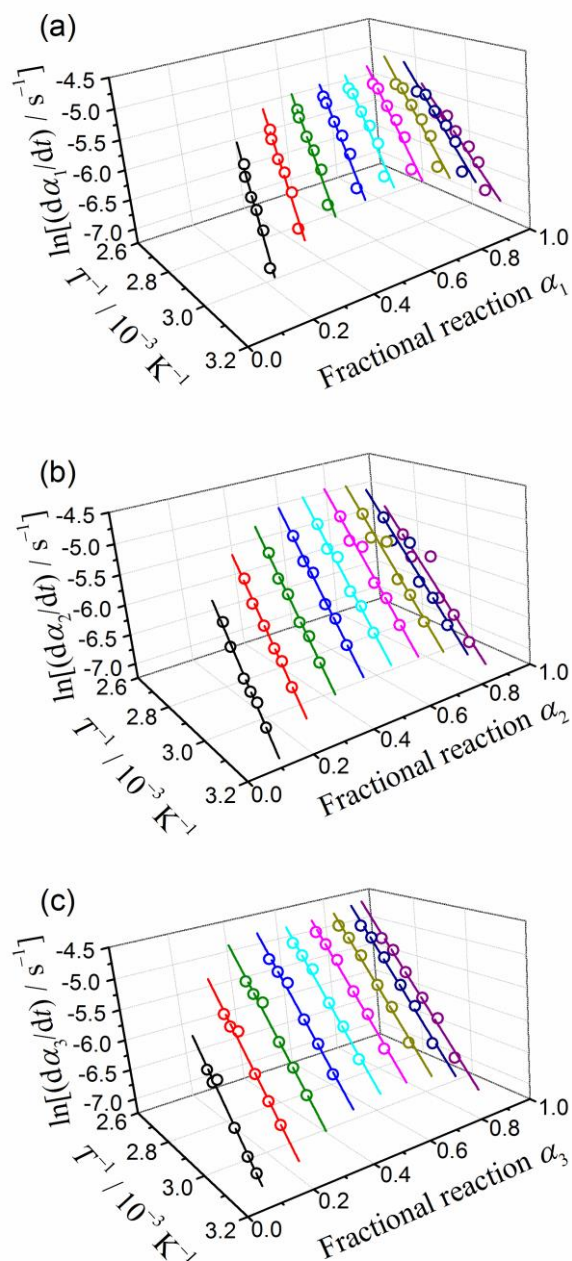


**Figure S5.** Friedman plots applied to the mathematically separated kinetic data for each reaction step of the thermal dehydration process: (a) first step, (b) second step, and (c) third step.

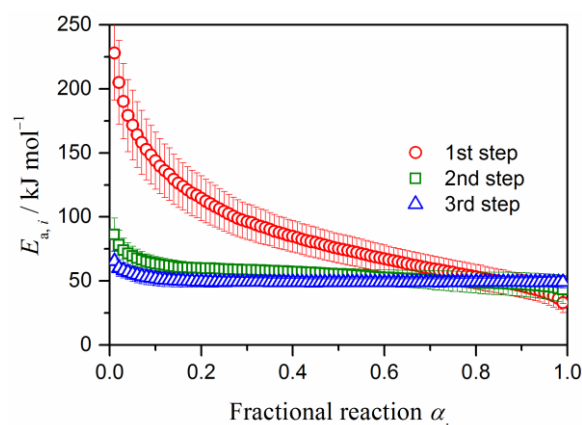


**Figure S6.**  $E_a$  values at different  $\alpha_i$  evaluated from the Friedman plots applied to the mathematically separated kinetic data for each reaction step of the thermal dehydration process.

For the reaction steps characterized by constant  $E_a$  values throughout, the rate behavior is simulated using the experimental master plots. The experimental master plot in differential form is drawn on the basis of eq. (S2).<sup>S3</sup>

$$\frac{d\alpha}{d\theta} = \left( \frac{d\alpha}{dt} \right) \exp\left(-\frac{E_a}{RT}\right) = Af(\alpha)$$

$$\text{with } \theta = \int_0^t \exp\left(-\frac{E_a}{RT}\right) dt \quad (\text{S2})$$

where  $\theta$  is Ozawa's generalized time,<sup>S4,S5</sup> denoting the hypothetical reaction time at infinite temperature calculated by extrapolating the reaction rate at each  $\alpha$  to infinite temperature according to the Arrhenius equation. Figure S7 shows the experimental master plots of  $(d\alpha/d\theta)$  versus  $\alpha$  for the second and third reaction steps. For the first reaction step, the further analysis using the experimental master plot is not theoretically correct. However, for empirical purposes, the experimental master plot was also drawn using the average  $E_a$  of  $73.8 \pm 18.7$  kJ mol<sup>-1</sup> ( $0.2 \leq \alpha \leq 0.9$ ). The experimental master plots for all the reaction steps reveal the maximum  $(d\alpha/d\theta)$  midway through each reaction step. The  $\alpha$  value at the maximum tends to increase for the latter reaction steps. The experimental master plot is correlated with  $f(\alpha)$  according to eq. (S2). An empirical  $f(\alpha)$ , i.e., the Šesták–Berggren model<sup>S6</sup> with three kinetic exponents, SB( $m, n, p$ ), was used for fitting the experimental master plots.

$$\text{SB}(m, n, p): f(\alpha) = \alpha^m (1-\alpha)^n [-\ln(1-\alpha)]^p \quad (\text{S3})$$

The empirical  $f(\alpha)$  has wide flexibility for fitting different types of physico-geometric reactions in the solid state and in deviated cases.<sup>S7, S8</sup> Through fitting the experimental master plots with SB( $m, n, p$ ), the most appropriate kinetic exponents that exhibit the best fit as shown in Figure S7 were determined by nonlinear least squares analysis using the Levenberg–Marquardt algorithm. The contribution and kinetic parameters ( $E_a$ ,  $A$ , and  $f(\alpha)$ ) determined for the mathematically separated kinetic data are summarized in Table S1.

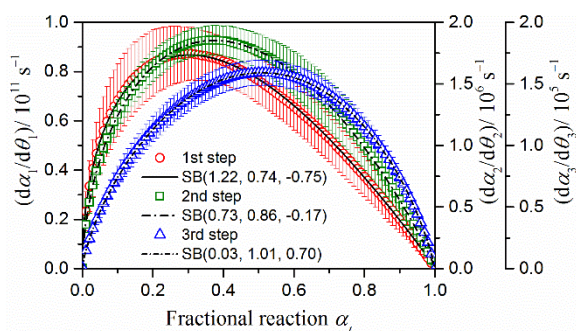


**Figure S7.** Experimental master plots of  $(d\alpha/d\theta)$  versus  $\alpha$  for the mathematically separated reaction steps  $i$  of the thermal dehydration process.

**Table S1.** Kinetic parameters for the respective reaction steps of the thermal dehydration process estimated through formal kinetic analysis for the mathematically separated kinetic data

$i$	$c_i$	$E_{a,i} / \text{kJ mol}^{-1}$	$A_i / \text{s}^{-1}$	$f_i(\alpha) = \alpha^m(1-\alpha)^n[-\ln(1-\alpha)]^p$		
				$m$	$n$	$p$
1	$0.10 \pm 0.01$	$73.8 \pm 18.7$	$(2.27 \pm 0.04) \times 10^{11}$	$1.22 \pm 0.12$	$0.74 \pm 0.04$	$-0.75 \pm 0.11$
2	$0.36 \pm 0.03$	$54.8 \pm 4.5$	$(5.00 \pm 0.04) \times 10^6$	$0.73 \pm 0.08$	$0.86 \pm 0.03$	$-0.17 \pm 0.03$
3	$0.54 \pm 0.03$	$49.1 \pm 0.6$	$(4.20 \pm 0.03) \times 10^5$	$0.03 \pm 0.05$	$1.01 \pm 0.02$	$0.70 \pm 0.05$

## S4. Kinetics of the thermal decomposition process

### S4-1. Kinetic data

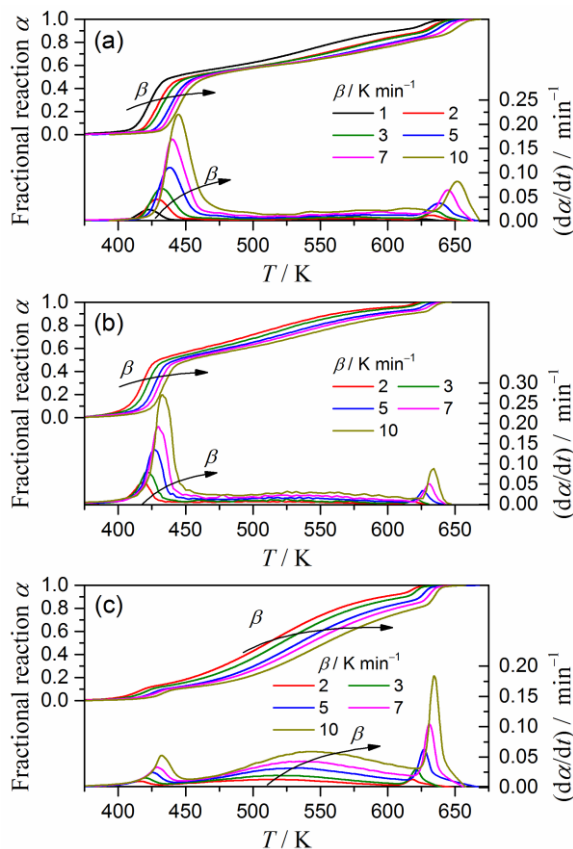
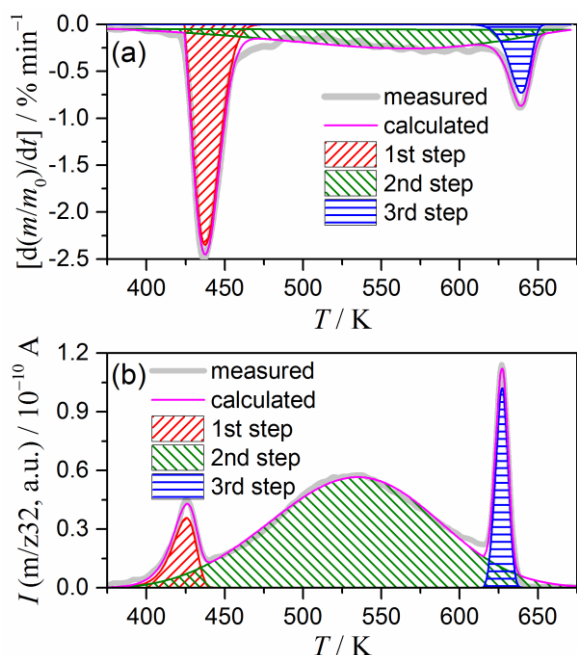


**Figure S8.** Kinetic data for the overall thermal decomposition of anhydrous SPB converted from (a) TG curves measured in  $\text{N}_2$  ( $80 \text{ cm}^3 \text{ min}^{-1}$ ), TG curves measured in  $\text{He}$  ( $200 \text{ cm}^3 \text{ min}^{-1}$ ), and (c) MS ion thermograms for  $m/z = 32$  measured in  $\text{He}$  ( $200 \text{ cm}^3 \text{ min}^{-1}$ ).

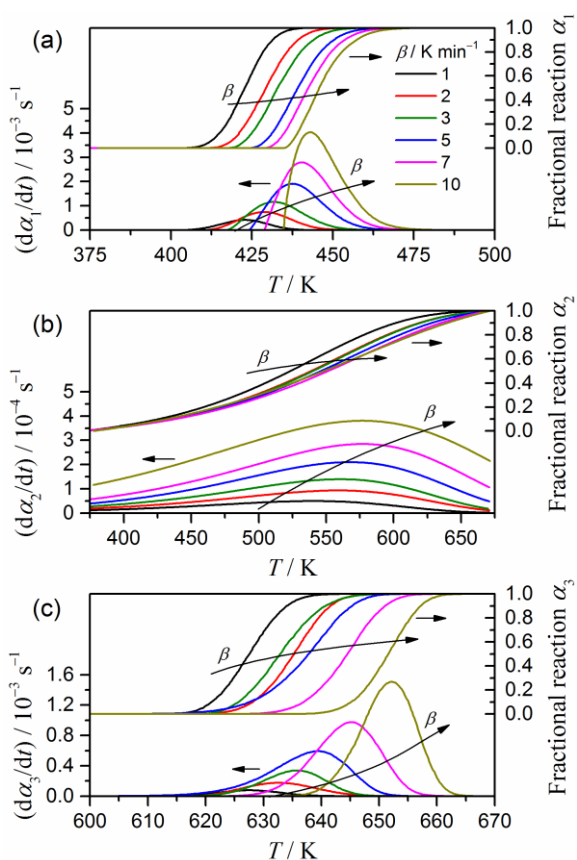
### S4-2. Mathematical deconvolution

Figure S9 shows typical results of the peak fitting using the Weibull function. The contributions of the component reaction steps estimated from the mathematical deconvolution of the kinetic data derived from DTG curves measured in flowing  $\text{N}_2$  (Figure S9a) were  $(c_1, c_2, c_3) = (0.43 \pm 0.01, 0.48 \pm 0.02, 0.09 \pm 0.02)$ . The contributions estimated from the kinetic data derived from the MS ion thermogram of  $m/z = 32$  in flowing  $\text{He}$  (Figure S9b) were  $(c_1, c_2, c_3) = (0.08 \pm 0.01, 0.82 \pm 0.04, 0.11 \pm 0.04)$ . The large difference in the contribution of the first reaction step between those kinetic data is apparently due to the different kinetic information traced by the DTG and the MS ion thermograms for  $m/z = 32$ , as aforementioned. However, a difference between those kinetic data is also seen for the ratio of  $c_2$  and  $c_3$ , where the ratio of the contribution of the second reaction step is apparently larger for the MS ion chromatogram data. A larger contribution by the second reaction step is also expected for the kinetic data derived from the DTG curves measured in flowing  $\text{He}$  from the wider  $\alpha$  region of the second reaction step with an approximately constant  $E_a$  value (Figure 13 in the main text). In addition to the large difference in the  $E_a$  values for the second reaction step evaluated from the kinetic data measured in flowing  $\text{N}_2$  and  $\text{He}$ , this observation on the second reaction step indicates the significant influence of the reaction atmosphere on the kinetic behavior.

Figures S10 and S11 show the kinetic curves of each reaction step of the thermal decomposition process obtained by the mathematical deconvolution analysis of the overall kinetic data derived from the DTG curves measured in flowing  $\text{N}_2$  and the MS ion thermograms for  $m/z = 32$  measured in flowing  $\text{He}$ , respectively. These kinetic curves systematically shift to higher temperatures with increasing  $\beta$ .



**Figure S9.** Typical results of the mathematical deconvolution of the DTG curves measured in flowing  $N_2$  ( $80 \text{ cm}^3 \text{ min}^{-1}$ ) and MS ion thermograms for  $m/z = 32$  measured in flowing He ( $200 \text{ cm}^3 \text{ min}^{-1}$ ) for the thermal decomposition process using Weibull function: (a) DTG curve at  $5 \text{ K min}^{-1}$  and (b) MS ion thermogram for  $m/z = 32$  at  $5 \text{ K min}^{-1}$ .



**Figure S10.** Kinetic data for each reaction step of the thermal decomposition process obtained by separating DTG curves measured in flowing  $N_2$  ( $80 \text{ cm}^3 \text{ min}^{-1}$ ) by the mathematical deconvolution using the Weibull function: (a) first step, (b) second step, and (c) third step.

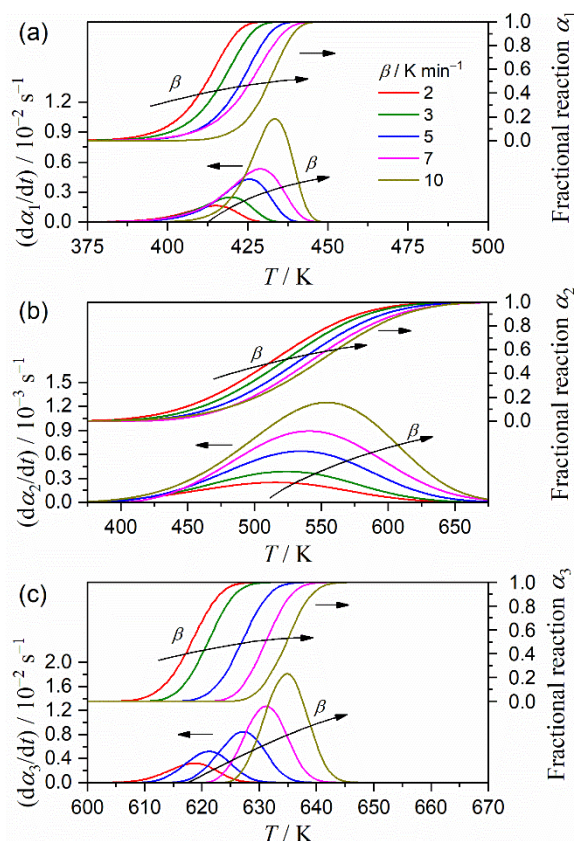


**Figure S11.** Kinetic data for each reaction step of the thermal decomposition process obtained by separating MS ion thermograms for  $m/z = 32$  measured in flowing He ( $200 \text{ cm}^3 \text{ min}^{-1}$ ) by the mathematical deconvolution using the Weibull function: (a) first step, (b) second step, and (c) third step.

### S4-3. Formal kinetic analysis

The apparent  $E_{a,i}$  values at different  $\alpha_i$  for each reaction step  $i$  were estimated from the mathematically separated kinetic curves using Friedman plots as shown in Figure S12. For all the reaction steps, systematic variations of  $E_{a,i}$  as the reaction advances were observed in both the values estimated from the separated kinetic curves from the DTG curves measured in flowing  $N_2$  and from the MS ion thermograms for  $m/z = 32$  in flowing He. The average  $E_{a,i}$  values in the range of  $0.1 \leq \alpha_i \leq 0.9$  in each reaction step  $i$  are listed in Table S2. The average  $E_{a,i}$  values for the first and third reaction steps are comparable for those evaluated from different data sources within the standard deviations. Conversely, the large discrepancy of  $E_{a,2}$  values between the different data sources recorded in flowing  $N_2$  and He is evidenced as has been seen in Figure 13. Because of the systematic variations of  $E_{a,i}$  values for all the reaction steps and for both the kinetic data sources, further kinetic treatment of the mathematically separated kinetic data using the master plot method was abandoned.

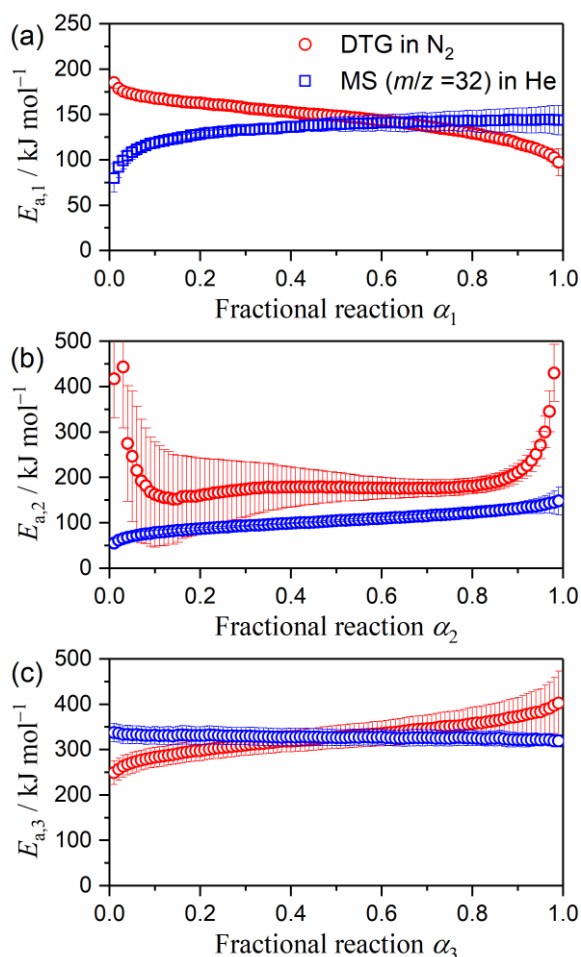


**Figure S12.** Variation of  $E_a$  evaluated from the Friedman plots applied to the mathematically separated kinetic data for each reaction step of the thermal decomposition process: (a) first step, (b) second step, and (c) third step.

**Table S2.** Average  $E_{a,i}$  values for each reaction step of the thermal decomposition process determined from the mathematically separated kinetic curves using the Friedman method

$i$	TG-DTG in $\text{N}_2$	MS ion thermogram ( $m/z=32$ ) in He
	$E_{a,i} / \text{kJ mol}^{-1}$	$E_{a,i} / \text{kJ mol}^{-1}$
1	$146.8 \pm 13.3$	$136.7 \pm 6.6$
2	$175.7 \pm 10.5$	$104.5 \pm 14.3$
3	$341.5 \pm 24.0$	$327.5 \pm 2.5$

**S4-4.** The first step of the thermal decomposition process

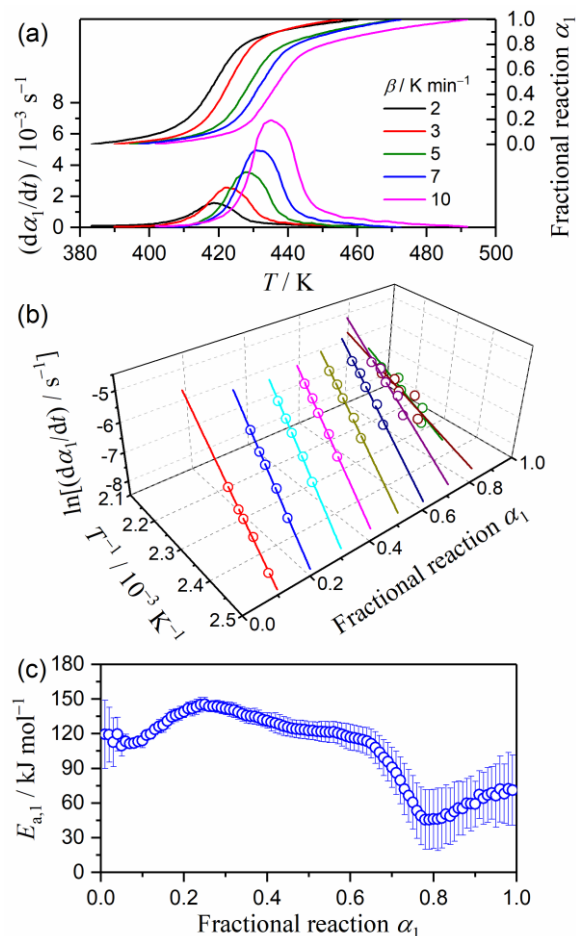


**Figure S13.** Kinetic analysis for the first reaction step of the thermal decomposition process using the MS ion thermograms for  $m/z = 18$ : (a) kinetic data converted from the MS ion thermograms for  $m/z = 18$ , (b) Friedman plots at different  $\alpha_1$ , and (c)  $E_{a,1}$  variation as the reaction advances.

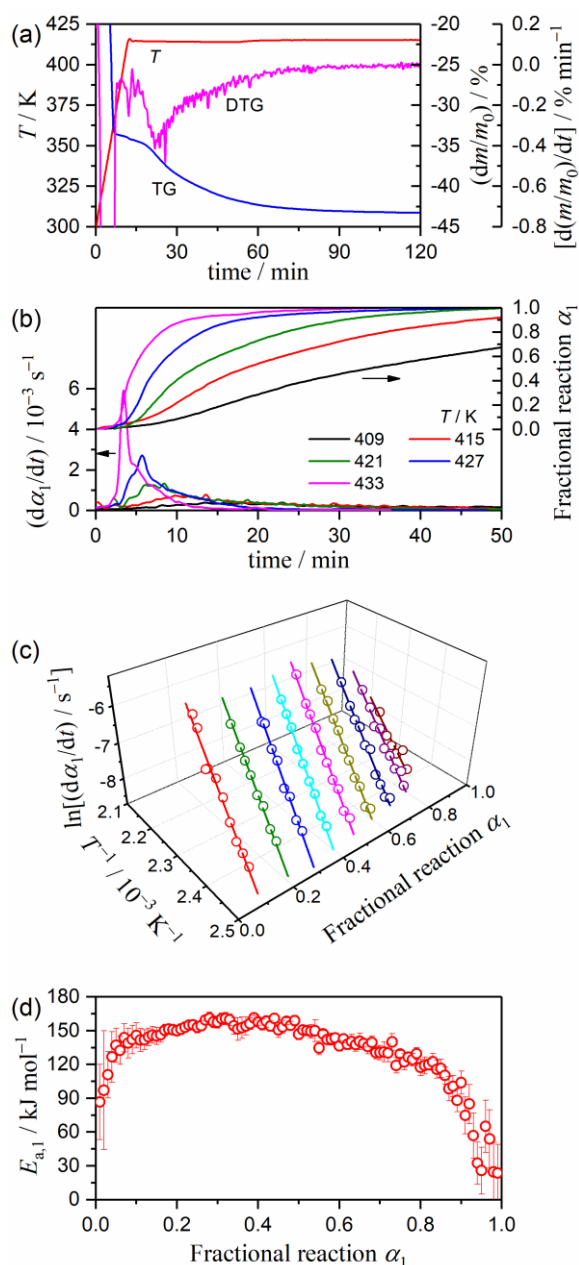


**Figure S14.** Kinetic analysis for the first reaction step of the thermal decomposition process using isothermal mass-change curves: (a) a typical isothermal mass-change measurement at 415 K, (b) kinetic data converted from the isothermal mass-loss curves (selected), (c) Friedman plots at different  $\alpha_1$ , and (d)  $E_{a,1}$  variation as the reaction advances.

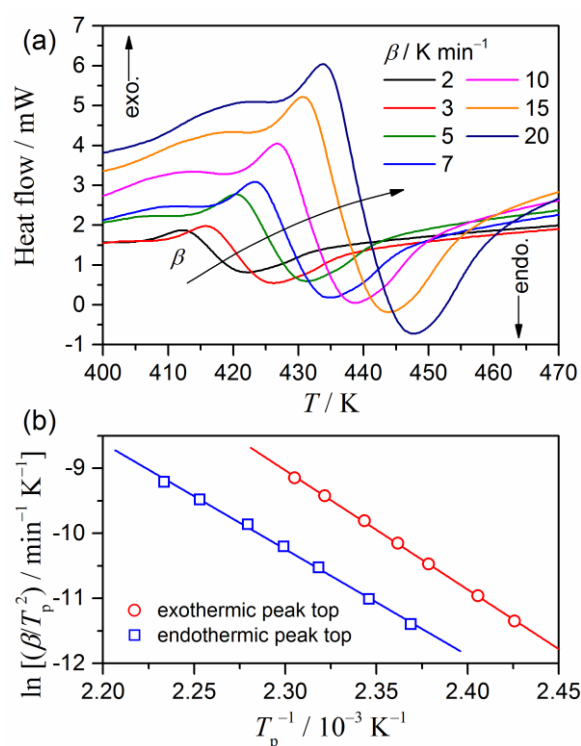


**Figure S15.** Thermal behavior during the first reaction step of the thermal decomposition process: (a) DSC curves at different  $\beta$  and (b) Kissinger plots applied to the exothermic and endothermic peak tops.

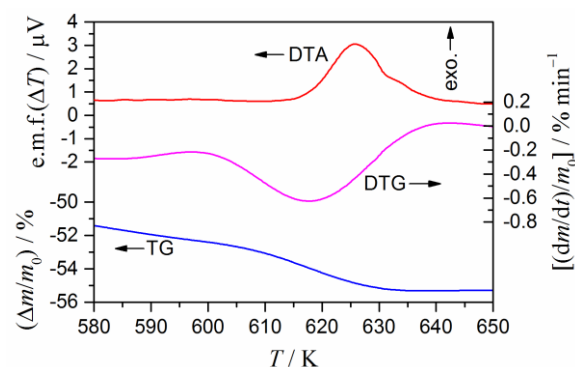


**Figure S16.** Typical TG–DTG–DTA curves for the third reaction step of the thermal decomposition process recorded for SPB-4AQ ( $m_0 = 5.020$  mg) at  $\beta = 5$  K min<sup>-1</sup> in flowing N<sub>2</sub> (80 cm<sup>3</sup> min<sup>-1</sup>).

## References

- S1. N. Koga, Y. Goshi, S. Yamada and L. A. Pérez-Maqueda, *J. Therm. Anal. Calorim.*, 2013, **111**, 1463-1474.
- S2. H. L. Friedman, *J. Polym. Sci., Part C*, 1964, **6**, 183-195.
- S3. F. J. Gotor, J. M. Criado, J. Málek and N. Koga, *J. Phys. Chem. A*, 2000, **104**, 10777-10782.
- S4. T. Ozawa, *Bul. Chem. Soc. Jpn.*, 1965, **38**, 1881-1886.
- S5. T. Ozawa, *Thermochim. Acta*, 1986, **100**, 109-118.
- S6. J. Šesták and G. Berggren, *Thermochim. Acta*, 1971, **3**, 1-12.
- S7. J. Šesták, *J. Therm. Anal.*, 1990, **36**, 1997-2007.
- S8. J. Šesták, *J. Therm. Anal. Calorim.*, 2011, **110**, 5-16.